

SCIENTIFIC REPORTS



OPEN

Determination of the endothelin-1 recognition sites of endothelin receptor type A by the directed-degeneration method

Seong-Gu Han¹, Sanghwan Ko¹, Won-Kyu Lee^{1,2}, Sang Taek Jung¹ & Yeon Gyu Yu¹

G-protein coupled receptors (GPCRs) play indispensable physiological roles in cell proliferation, differentiation, and migration; therefore, identifying the mechanisms by which ligands bind to GPCRs is crucial for developing GPCR-targeting pharmaceuticals and for understanding critical biological functions. Although some structural information is available regarding the interactions between GPCRs and their small molecule ligands, knowledge of how GPCRs interact with their corresponding macromolecule ligands, such as peptides and proteins, remains elusive. In this study, we have developed a novel strategy to investigate the precise ligand recognition mechanisms involved in the interaction of endothelin receptor type A (ET_A) with its ligand, endothelin-1 (ET-1); we call this method “directed degeneration” method. Through flow cytometric screening of a randomized ET_A library, statistical analysis of the identified sequences, and biochemical studies, the ligand interaction map was successfully obtained.

G-protein coupled receptors (GPCRs) are the largest membrane protein family; they regulate various crucial physiological processes, including cell migration, differentiation, and proliferation, by delivering extracellular signals into the interior of the cell by triggering the activation of G-protein heterotrimers^{1–3}. The signaling cascade of a GPCR is initiated by binding to its ligand. Therefore, identifying the ligand recognition mechanisms of GPCRs is crucial for facilitating drug discovery processes as well as elucidating signal cascades. Understanding the thermodynamics of binding of a ligand to a target GPCR, for example, has guided the development of new drugs by rational approaches^{4–12}. Furthermore, several reports have suggested that optimization of the ligand binding enthalpy may address ADME issues (adsorption, distribution, metabolism, and excretion of a drug)^{10–13}. Dozens of GPCR complex structures with small molecule ligands have revealed how GPCRs recognize small molecule ligands¹⁴; these structures indicate that the binding pockets of small molecule ligands are located in the transmembrane regions (TMs) of GPCRs. However, the binding mechanism of native macromolecule agonists, such as endothelin-1 (ET-1) and Wnt to their corresponding GPCRs remains elusive.

Human endothelin receptor type A (ET_A) is a Class A (rhodopsin-like) GPCR that is involved in vasoconstriction *via* a G_{αq} signaling cascade triggered by binding its native peptide agonist, ET-1¹⁵. Recently, the correlation between ET_A and the progression of various cancers by increasing metastatic potential and proliferation has been validated^{3,16–18}. Furthermore, the expression of endothelin receptors in cancer cells reduces patient survival rate by promoting cancer malignancy¹⁹. Due to this close relationship between ET_A and tumor malignancy, ET_A is an attractive cancer drug target. For example, bosentan, a drug currently available on the market that targets endothelin receptors for pulmonary arterial hypertension, has been re-developed for the treatment of melanoma³. Therefore, understanding the ligand recognition of ET_A is highly important to facilitate the development of drugs targeting ET_A as well as to understand the signal cascades of the receptor.

The ET-1 binding sites of ET_A have been studied using mammalian cells expressing chimeric ET_A^{20,21} as well as by molecular modeling^{22–24}. However, the results are ambiguous, or the binding sites are too localized to explain the global binding mode of ET-1 against ET_A. For example, Wallace and his colleagues showed that ET-1 binds

¹Department of Chemistry, Kookmin University, 861-1 Jeongneung-dong, Seongbuk-gu, Seoul, 136-702, Republic of Korea. ²New Drug Development Center, Osong Medical Innovation Foundation, Osong Sengmyung-Ro 123, Osong-eup, Heungdeok-gu, Cheongju-si, Chungbuk, Republic of Korea. Correspondence and requests for materials should be addressed to S.T.J. (email: sjung@kookmin.ac.kr) or Y.G.Y. (email: ygyu@kookmin.ac.kr)

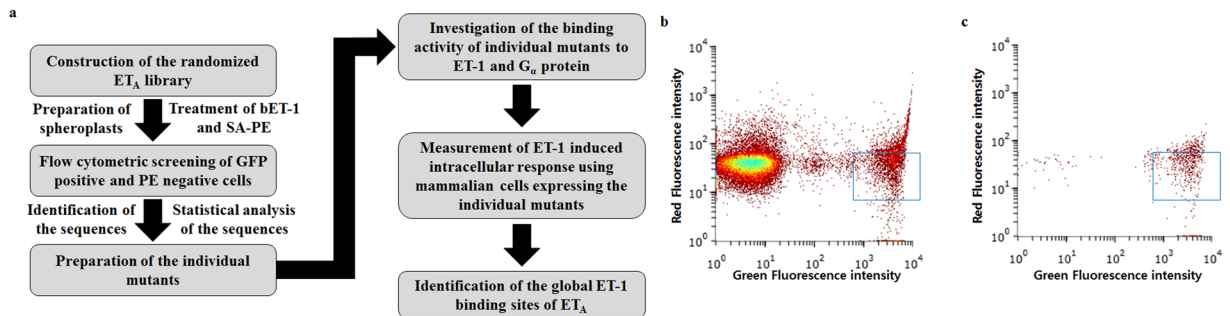


Figure 1. The directed degeneration method and flow cytometric screening of the ET_A library. **(a)** Flow chart of the directed degeneration method. After construction of the ET_A library by random mutagenesis, the spheroplasts expressing the library were treated with bET-1 and SA-PE, followed by isolation of the GFP-positive and PE-negative clones using FACS. After sequence analysis of the isolated clones, the P9-ET_As harboring these mutations were prepared, and their binding affinities to ET-1 were characterized. Also, the effects of the isolated mutations on ET-1-dependent signaling were confirmed in CHO-K1 cells expressing the ET_A mutants. Through biochemical and cell-based studies, the ET-1 interaction map of ET_A was successfully generated. **(b and c)** Histograms showing the first round **(b)** and the second round **(c)** of FACS screening of the ET_A library. The blue squares in the histograms indicate gating regions. In the first and the second rounds of sorting, approximately 10⁶ spheroplasts comprising 4% and 1.4% of the total population were collected.

to the extracellular domain of ET_A according to their molecular model²², whereas Rao *et al.* suggested that the transmembrane domain of ET_A is the ET-1 binding pocket²³. Therefore, a precise and global ET-1 interaction map of ET_A is necessary to understand the ET-1 recognition mechanism.

Recently, we established an *E. coli* expression system of ET_A by N-terminus fusion of P9, which is an envelope protein of *Pseudomonas phi6*, and an amphipathic polymer that can stabilize membrane proteins in their functional conformation; these are called the P9 expression system and amphipathic poly- γ -glutamic acid (APG), respectively^{25–28}. Although the ET_A had N-terminal P9-tag without glycosylation, the protein showed specific and selective binding activities with its ligand and G_α proteins indicating that this system should be appropriate for screening of ET_A variants for ET-1 binding. With these methods, we identified the precise ET-1 binding mechanism of ET_A with a novel biochemical strategy called the “directed degeneration” method as shown in Fig. 1a. First, we generated a randomized ET_A library by error-prone PCR. We then screened the degenerative clones using fluorescence activated cell sorting (FACS) to isolate the clones that had lower ET-1 binding activity compared to wild type ET_A and had no internal stop codon. Through statistical sequence analysis of the isolated clones followed by biochemical analysis of the purified ET_A mutants, the ET-1 interaction map of ET_A was successfully obtained. The effects of these mutations on intracellular signaling were finally confirmed by measuring ET-1 induced variations of intracellular Ca²⁺ levels using mammalian cells expressing the mutants. Here, we demonstrate that the extracellular N-terminus region and the entrances of the third and seventh transmembrane helix of ET_A are involved in the interaction with ET-1.

Results

Construction of a randomized ET_A library and isolation of ET_A variants exhibiting reduced binding to ET-1. Through randomization of ET_A and fusion of P9 and green fluorescence protein (GFP) at the N-terminus and C-terminus, respectively, an ET_A library composed of approximately 10³ diverse ET_A variants was successfully constructed. As shown in Supplementary Table S1, the average mutation number per clone was approximately 5.9. Considering the size of the ET_A (2 to 427) gene (1278 bp) and the average mutation number per clone, the error rate of the library was estimated to be 0.46%; this is in good agreement with the desired error rate of the error-prone PCR step (0.5%).

After cultivation of the library, the outer membrane and peptidoglycan layer of the cells, expressing the randomized ET_A fused with P9 and GFP at the N-terminus and C-terminus, respectively, were removed; the resulting spheroplasts were sequentially incubated with 0.5 μ M C-terminally biotinylated ET-1 (bET-1) and 10 nM phycoerythrin (PE)-conjugated streptavidin (SA-PE). The spheroplasts that exhibited positive GFP fluorescence due to the absence of an internal stop codon and negative PE fluorescence due to their low ET-1 binding activity were selectively collected by two flow cytometry sorting processes (Fig. 1b and c). As shown in Fig. 1b, a substantial portion of the ET_A library showed very low GFP signals, suggesting that these clones may have internal stop codons resulting from random mutagenesis during the library construction. Through the first round of sorting, the cells that showed high GFP signals and low PE signals, representing approximately 4% of the total applied cells (Fig. 1b, boxed region), were isolated. The results of the subsequent sorting round showed that most of the clones with low or mid-range GFP signals and high PE signals were successfully eliminated (Fig. 1c). Through the second sorting, approximately 10⁶ GFP-positive and PE-negative cells, representing 35% of the first isolated cells and 1.4% of the total cells, were recovered.

Statistical sequence analysis of the isolated clones. After TA cloning of the isolated clones using the pGEM-T vector, the sequences of 20 different plasmids selected during white colony screening were analyzed using T7 and SP6 promoter primers (Supplementary Table S1). The sequences of 19 clones were analyzed; clone

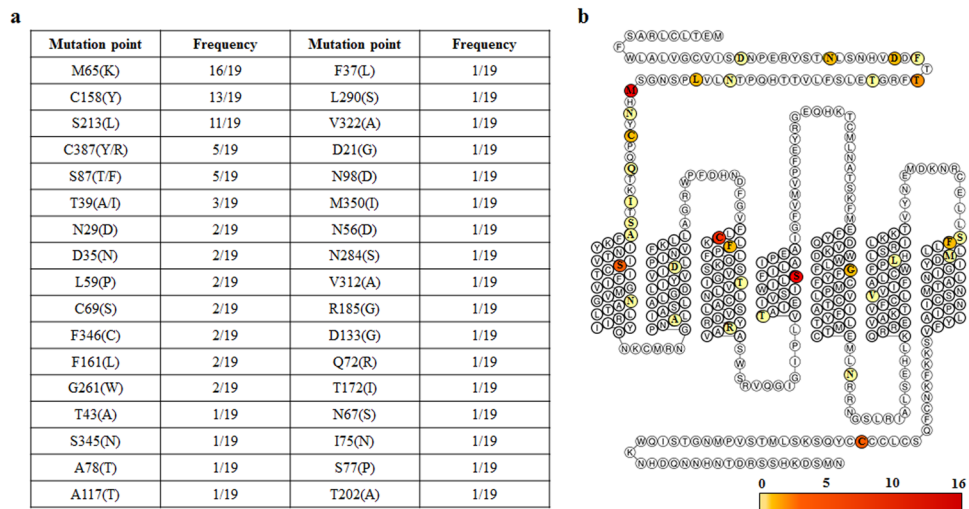


Figure 2. Statistical sequence analysis of the isolated clones and snake plot of the identified mutation points of ET_A. **(a)** The mutations observed in the isolated clones are listed according to their frequencies. **(b)** Snake plot of the isolated mutation points of ET_A. The colors of the circles indicate the frequency of mutation (Fig. 2a), as represented at the bottom with scale bar.

number 20 was not sequenced due to failure of the sequence analysis (data not shown). Clone number 7 and 13 were confirmed to be the same clone. And the 34 mutation points were confirmed *via* statistical analysis of the sequencing results, and 13 mutation points were appeared at least twice (Fig. 2a). As shown in Fig. 2b, these mutation points, which may influence the binding of ET-1, are represented in the snake plot of ET_A (www.gpcrdb.org). More than half of these mutations were located at the extracellular N-terminus region and the entrance region of TM3 and TM7 (Fig. 2b). The remaining mutations were widely spread in the TM regions or in the intracellular domains.

Investigation of ET-1 binding activities and structural integrities of the individual P9-ET_A mutants.

To examine the effects of the identified mutations on their interactions with ET-1, ET_A mutants containing each identified mutation were prepared and their direct interactions with ET-1 were evaluated. We selected 12 mutation sites which appeared more than twice and were located at the extracellular or transmembrane regions for further study. The C387 mutation, which was observed five times in the mutants, was not included for further study because the mutation site was located in the intracellular region. The individual mutants composed of N29D, D35N, T39A, L59P, M65K, C69S, S87F, S87T, C158Y, F161L, S213L, G261W, and F346C were expressed in *E. coli* using a P9-fusion system, and their expression levels were determined (Fig. 3a). Among them, mutations that resulted in low expression (S87F; Fig. 3a) or inclusion body formation (T39A and C158Y; Fig. 3b) were not examined further. Wild type P9-ET_A and 10 different mutants, including K140I, which has been identified to be involved in ET-1 binding^{20,21}, were successfully expressed and purified (Supplementary Figs S1–S6).

We then reconstituted the proteins with APG, which was synthesized by the conjugation of alkyl and glucosyl groups to the carboxylic acid groups of poly- γ -glutamic acid and which facilitates the stabilization of P9-ET_A in its active conformation^{27,28}. Then, the ET-1 binding activities of the mutants compared to wild type P9-ET_A were investigated (Fig. 3c). To measure the relative binding activities of the purified proteins to ET-1, we applied 5 μ M ET-1 to the immobilized proteins; this concentration is sufficient to cover the maximal binding capacity (B_{max}) of the receptors because it is about 100-fold higher than the apparent equilibrium dissociation constant (K_D) of the wild type P9-ET_A complex with APG against ET-1 (60 nM)²⁷. As shown in Fig. 3c, all the mutants except S213L showed reduced binding to ET-1 compared to wild type P9-ET_A. The control mutant containing the previously identified K140I mutation showed significantly reduced interaction with ET-1, suggesting that our system worked well as designed and that the identified mutation sites, except S213L, were involved in the interaction with ET-1. Notably, the M65K mutation, which was observed with the highest frequency in the sequence analysis (Fig. 2a), showed the lowest binding activity with ET-1.

It is possible that these mutations destabilize the native conformation of ET_A and that the reduced interaction with ET-1 results from conformational defects rather than direct involvement of the mutations in ET-1 binding. To examine the structural integrity of these mutant proteins, the interactions between the mutants and G_{o13} were measured. The canonical signaling cascade triggered by ET-1 is mediated by G_{oq}²⁹. However, purified ET_A and ET_A expressed in mammalian cells can interact with various G_o proteins including G_{o13}^{30,31}. Therefore, we investigated whether the selected mutations affected the structural integrity of the protein by measuring the binding activities of the mutants to G_{o13} compared to wild type P9-ET_A. As shown in Fig. 3d, all the mutants showed similar or almost identical binding activities to the G_{o13} protein compared to wild type P9-ET_A, indicating that these mutations directly reduced the affinity to ET-1 rather than inducing structural distortions.

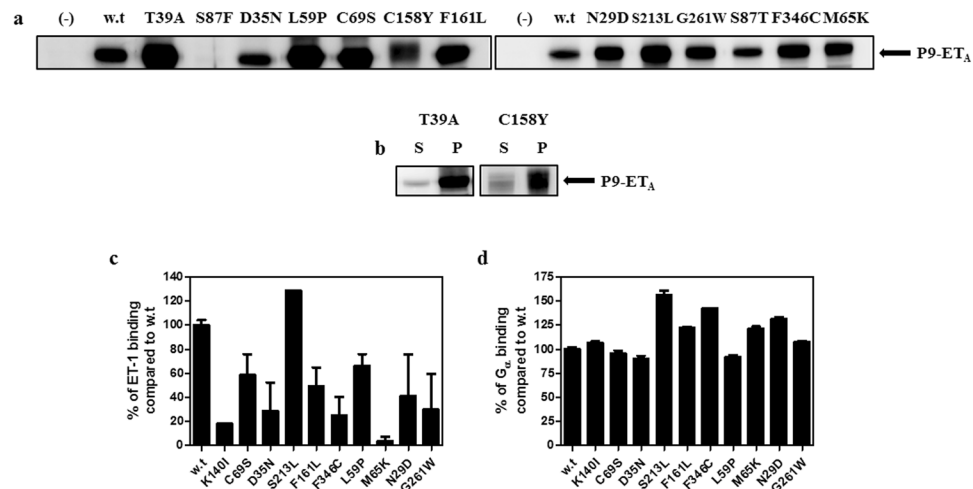


Figure 3. Expression of the individual mutants and the relative affinities of the mutants against ET-1 and G_{oi3} . **(a)** Western blot analysis of the crude extracts from *E. coli* expressing P9-ET_A harboring each single amino acid substitution using anti-P9 antibodies. The lanes are described as follows. (-): crude extract prior to induction, w.t: crude extract of wild-type after induction, others: crude extracts of indicated mutants after induction. The full-length blots are represented in Supplementary Figure S8. **(b)** Western blot analysis of the supernatant (S) and pellet (P) fractions after centrifugation of cell lysates expressing T39A and C158Y mutants. The full-length blots are represented in Supplementary Figure S9. **(c)** ET-1 binding activities of the mutants compared to wild type P9-ET_A. The purified mutants were analyzed for their ET-1 binding activities using 5 μ M bET-1 and SA-HRP. “w.t” represents wild type P9-ET_A, and the others represent the indicated mutants of P9-ET_A. The error bar represents the standard error of the mean (SEM). **(d)** G_{oi3} binding activities of the mutants compared to the wild type. The interactions between the mutants and immobilized G_{oi3} were analyzed using 1 μ M mutant and anti-P9 antibody. “w.t” represents wild type P9-ET_A, and the others represent the indicated mutants of P9-ET_A. The error bar represents the SEM.

Influences of the mutations on the intracellular response. The reduced affinity of ET_A to ET-1 for the identified mutations suggests that these mutations may retard ET-1-dependent intracellular signaling, such as the G_q signaling cascade. Signal transduction *via* G_q , the major ET-1 stimulating signal cascade of ET_A, accompanies the increment of cytosolic Ca^{2+} levels through Ca^{2+} release from the endoplasmic reticulum (ER) *via* the inositol-1,4,5 triphosphate (IP₃) receptor²⁹. To examine the effects of the mutations on the ET-1-dependent signaling cascade, we used a cytosolic Ca^{2+} -sensitive fluorescent dye, Fura-2-AM, to measure the ET-1 dependent change of the intracellular Ca^{2+} levels of CHO cells that transiently expressed wild type or mutant ET_As. As shown in Fig. 4a, all the cells expressing the mutants showed notably decreased cytosolic Ca^{2+} concentrations compared to cells expressing wild type ET_A after stimulation by treatment with 1 μ M ET-1. The effect of the K140I mutation appeared to be the most dramatic because the cytosolic Ca^{2+} level was almost identical to the level of naïve CHO cells after stimulation with ET-1 treatment. The cells expressing the F346C, L59P, M65K, and F161L mutants showed 80% to 90% decreased Ca^{2+} response compared to the cells expressing wild type ET_A; the D35N, C69S, and N29D mutants exhibited 50% to 60% decreased Ca^{2+} response. The mRNA levels of mutated ET_A in the transformed CHO cells, measured by real-time PCR, were almost identical to the wild type ET_A expressing cells (Fig. 4b). Furthermore, the protein expression levels of ET_A variants in the transformed CHO cells were almost identical likewise the identical mRNA levels indicating that the mRNA levels are directly correlated with the expression levels of the proteins in the transformed CHO cells (Supplementary Fig. S7). These results indicated that the mutations that have reduced affinity to ET-1 also show retarded ET-1-dependent signaling.

Discussion

In this study, we developed a biochemical strategy to identify the ET-1 binding sites of ET_A by a protein engineering method called “directed degeneration”. The ET_A variant library was successfully constructed using standard error-prone PCR (error rate: 0.46%). Through flow cytometric screening of the ET_A library on the basis of the fluorescence signals derived from GFP fusion at the C-terminus of ET_A, and through binding of biotinylated ET-1 followed by streptavidin-PE labeling, GFP-positive and PE-negative clones possessing no internal stop codon and low binding activity to ET-1 were isolated. DNA sequencing of the selected clones revealed 34 mutation points that potentially affected ET-1 recognition. Among them, 13 mutation points were observed repeatedly, suggesting significant roles of these mutations in ET-1 binding. Particularly, the M65K mutation appeared in 16 out of 19 clones. Individual ET_A mutants with each identified mutation, except for T39, S87, C158, and C387, were successfully expressed and purified along with the K140I mutant.

Nine of ten mutant ET_As (N29D, D35N, L59P, M65K, C69S, K140I, F161L, G261W, and F346C) showed considerably reduced ET-1 binding activities compared to wild type ET_A. Furthermore, the mutants likely have no significant structural distortions because they had very similar or slightly higher G_{oi3} binding activities compared to wild type ET_A. To investigate the quantitative rate constants (k_a and k_d) and the K_D of ET-1 for the ET_A variants

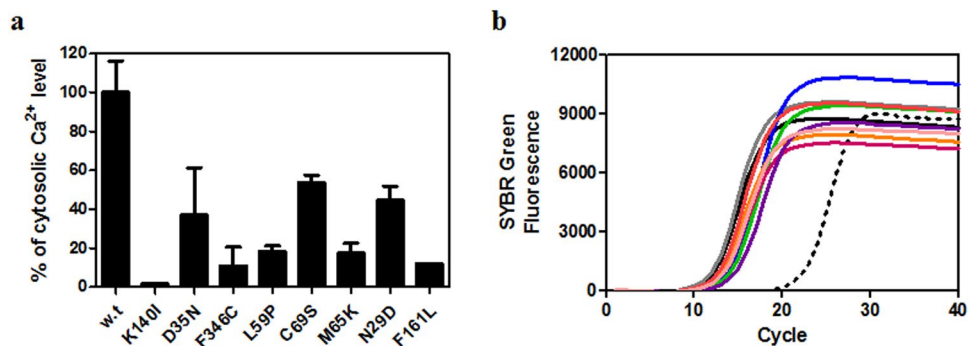


Figure 4. Measurement of cytosolic Ca²⁺ levels. **(a)** Measurement of cytosolic Ca²⁺ levels of CHO-K1 cells expressing wild type and mutant ET_A after treatment with ET-1. After transient expression of the mutants in the CHO-K1 cell line by transfection of the pCMVTag3B vector including each mutant as well as wild type ET_A, the cells were incubated with 5 μM Fura-2-AM followed by incubation with 1 μM ET-1. The cytosolic Ca²⁺ level was estimated by measuring the ratio of the fluorescence intensities emitted at 510 nm at two distinct excitation wave-lengths, 340 nm and 380 nm. The percentage was calculated based on the ratio of wild type ET_A as 100% and the ratio of CHO-K1, which is not transfected, as 0%. “w.t.” represents wild type ET_A, and the others represent the indicated mutants of ET_A. The error bar represents the SEM. **(b)** RT-PCR of cDNA from transfected CHO-K1 cells. After preparation of the total RNA from CHO-K1 cells harboring each mutant and wild type ET_A, cDNA was obtained by reverse-transcription PCR using ET_A gene-specific primers. The cDNA was amplified by PCR reaction with SYBR green dye, and the SYBR green fluorescence signals of amplified DNA from non-transfected CHO-K1 (black dotted line), CHO-K1 harboring wild type ET_A (black solid line), K140I (gray line), N29D (blue line), D35N (green line), L59P (orange line), M65K (red line), C69S (magenta line), F161L (violet line), and F346C (pink line) were recorded in each PCR cycle.

compared with wild type ET_A, surface plasmon resonance (SPR) experiments were carried out using XPR36 (Bio-Rad, USA) equipment. In the SPR experiments, P9-ET_A was immobilized very poorly on sensor chips functionalized with nitrilotriacetic acid (NTA) or carboxymethyl (CM) groups (data not shown). We believe that these immobilization problems may derive from steric hindrance of the poly-histidine tag at the C-terminus and the low accessibility of carboxymethyl groups to the exposed lysine residues.

One mutation (G261W) that showed reduced affinity to ET-1 substituted glycine for tryptophan in the center of the fifth transmembrane helix (TM5), as depicted in Fig. 2b. This substitution may directly affect the interaction with ET-1. Alternatively, the Trp substitution may affect the structure of ET_A by disturbing the compactness of the transmembrane helices by decreasing the degree of structural freedom and increasing the occupied space, thereby reducing the affinity of ET_A against ET-1. Likewise, the C69S mutation was assumed to destabilize ET_A because this substitution prevents the formation of a disulfide bridge with C341 at extracellular loop 3 (ECL3)²⁴. We propose that the C69S and G261W mutants destabilized the structure of ET_A, resulting in low binding affinity to ET-1. Identification of the C69S and G261W mutants by this strategy provides further evidence that the “directed degeneration” method is effective to identify mutations that affect ligand binding as well as mutations that destabilize protein structures.

It is confirmed that the six novel mutations (N29D, D35N, L59P, M65K, F161L, and F346C) decreased the binding of ET-1 and also inhibited downstream signaling of ET_A stimulated by ET-1 in mammalian cells. The newly identified ligand binding sites of ET_A in this study and the amino acids identified by previous reports are represented in Fig. 5^{20,21}. It should be noted that several amino acids in the extracellular N-terminus domain of ET_A were first identified as crucial residues for ET-1 binding. Additionally, F161 and F346, which are critical for the interaction with ET-1, are located at the entrance regions of TM3 and TM7, respectively, similarly to K140 (entrance of TM2). Considering the high solubility of the ET-1 peptide (>1 mg/mL), our results indicate that the binding site of ET-1 is mainly located in the extracellular domain of ET_A. Recently, a crystal structure of endothelin receptor type B (ET_B), which lack the N-terminus region (1–87 amino acids), complex with ET-1 has been reported³². In this structure, the extracellular region of ET_B is widely involved in ET-1 binding, which is in good agreement with our results. The three C-terminus residues of ET-1 (I19, I20, and W21) bind to the hydrophobic pocket of ET_B consisted of I157 (TM2), P178 (TM3), V185 (TM3), F240 (ECL2), L277 (TM5), W336 (TM6), L339 (TM6), and Y369 (TM7). The F161 (TM3) and F346 (TM7) of ET_A which are identified as ET-1 binding sites of ET_A are correspond to the P178/V185 and Y369 of ET_B, respectively, and they might form hydrophobic ET-1 binding pocket likewise ET_B. Although the structure of ET_B with ET-1 could not provide a precise role of the N-terminus domain in ET-1 binding, the amino acids in the N-terminus domain of ET_B, which are correspond to the amino acids (N29, D35, L59, and M65) of ET_A, which are identified as ET-1 binding sites in this study, may have an important role to recognize ET-1.

The “directed degeneration” method is distinct from previous biochemical approaches^{20,21}, which focus on localized regions for mutagenesis study; this is because our method introduces random mutations in any part of the protein, and mutants with decreased binding affinity to the ligand are selected. Therefore, the strategy of this study provided a novel recognition mode of ET_A against its ligand. Structural investigation has provided much valuable information about protein including ligand interaction modes; however, the exact structural information

supplemented with 100 µg/mL of ampicillin in a square plate. The mutation rate of the constructed library was analyzed by DNA sequencing.

Flow cytometric screening. *E. coli* BL21(DE3) cells harboring plasmids for ET_A variants were inoculated into 100 mL of LB media containing 100 µg/mL ampicillin. The cells were grown at 37 °C until the OD_{600nm} reached 0.5 to 0.6, followed by induction at 25 °C for 4 h with 0.5 mM IPTG. After harvesting the cells by centrifugation at 5,000 × g for 20 min, spheroplasts were obtained by osmotic shock and lysozyme treatment as previously described³⁵. The resulting spheroplasts were incubated with 0.5 µM bET-1 at room temperature for 1 h, washed with PBS, and subsequently incubated with 10 nM SA-PE under the same incubation conditions. After washing, the fluorescently labeled spheroplasts were analyzed by flow cytometry (S3 cell sorter, Bio-Rad, USA) and cell populations displaying high GFP signals and low PE signals were sorted.

TA cloning of the isolated clones. The sorted spheroplasts were re-cloned with the pGEM-T vector for sequence analysis. ET_A genes in the isolated clones were amplified by PCR using a primer set (5'-tgccgcgctccggcggaacccttgcctcagggc-3' and 5'-ttaatggtgatggtgatggtgagaa gctctgtcatgctgtcttatgctgc-3') and Hot Start *Taq* polymerase. After the PCR products and pGEM-T Easy Vector were ligated by incubating at 4 °C over-night with T4 DNA ligase, the reaction mixture was transformed into *E. coli* (DH5α strain) and spread on a LB agar plate containing 100 µg/mL ampicillin, 0.5 mM IPTG, and 80 µg/mL X-gal.

Statistical sequence analysis of the isolated clones. After TA cloning of the isolated clones, the sequences of 20 different plasmids selected during white colony screening were analyzed using T7 and SP6 promoter primers. Based on the sequences of 19 clones (clone number 20 was not sequenced due to failure of the sequence analysis (data not shown)), the appeared each single mutation was statistically arranged by the frequency.

Site-directed mutagenesis. Site-directed mutagenesis was performed to generate individual P9-ET_A mutants by PCR using wild-type pP9-ET_A as a template and the primer set described in Supplementary Table S2, followed by incubation with *DpnI*. It was confirmed by sequence analysis that the C158Y, S87F, D35N, and N29D mutants were successfully generated; other mutants, however, were not successfully generated. To address this problem, we designed new primer sets using conventional mutagenesis method involving two-step PCR containing K140I, a common mutant identified in a previous study^{20,21}, to use as a control mutant as described in Supplementary Table S3. The first and second fragments were amplified by PCR using the T7 promoter primer/Frag1 Rv primer set and the Frag2 Fw/T7 terminator primer set, respectively. The two DNA fragments were assembled by PCR using the T7 promoter and T7 terminator primer. The PCR products were inserted into the linearized pP9 vector by *HindIII* digestion using the Gibson cloning method. The sequences of the mutants were analyzed using the T7 promoter and T7 terminator primers.

Preparation of P9-ET_A wild-type and mutants. Expression and purification of the P9-ET_A wild type and mutants were performed as described previously²⁵. Briefly, expression of the wild type and mutants in *E. coli* BL21(DE3) strain was induced by the addition of 0.5 mM IPTG when the optical density of the culture at 600 nm reached 0.5 to 0.6. After induction, the cells were incubated at 25 °C for 4 h and harvested by centrifugation. The cell pellets from 1.0 L of culture were resuspended in 20 mL of buffer A (25 mM Tris-HCl, pH 7.8) containing 1 mM PMSF, and the cells were lysed using an M-110P microfluidizer (Microfluidics, USA). Cell debris was removed from the lysate by centrifugation at 12,000 × g for 20 min before the membrane fraction was recovered by ultracentrifugation at 100,000 × g for 1 h. The pellet containing the membrane proteins was homogenized with buffer B (0.5% sarkosyl in buffer A) at 4 °C for 3 h, and the insoluble materials were removed by centrifugation at 30,000 × g for 30 min. The supernatant containing solubilized membrane proteins was loaded onto a Ni-NTA agarose column that was pre-equilibrated with buffer B. After washing the column with 20 mM imidazole in buffer B, the bound proteins were eluted with 300 mM imidazole in buffer B. The buffer of the eluted protein fraction was exchanged with buffer B using a PD-10 desalting column (GE, USA) to remove excess imidazole. The prepared proteins were stabilized in their active conformation with APG as previously described^{27,28}. The proteins were stored with 10% glycerol at -80 °C until further use.

ELISA for ET-1 binding activity of the mutants. 5 µg of each of the P9-ET_A wild-type and mutants were immobilized on a 96-well medium binding plate (Corning, USA) by incubating at room temperature for 2 h. After extensive washing, each well was blocked with 5% (w/v) skim milk followed by incubation with 5 µM bET-1 at room temperature for 2 h. After extensive washing, the amount of bET-1 bound with the ET_A variant was estimated by color development using SA-HRP and TMB; then 2.5 N H₂SO₄ was added to quench the reaction. The absorption at 450 nm of each well was measured using a multi-plate reader (Triad multimode detector, DYNEX Technologies, USA).

ELISA for G_{αi3} binding activity of the mutants. After G_{αi3} protein was prepared as previously described³⁶, 1 µg of G_{αi3} was immobilized on each well of a 96-well medium binding plate by incubating at room temperature for 2 h. After blocking the vacant space of each well with 5% skim milk, 1 µM of each mutant and the P9-ET_A wild type were treated and incubated at room temperature for 2 h, followed by extensive washing. Anti-P9 and HRP-conjugated anti-mouse antibody were sequentially incubated at room temperature for 1 h. After extensive washing, the amount of P9-ET_A was measured by color development of TMB. The reaction was quenched by adding 2.5 N H₂SO₄ and the absorption at 450 nm of each well was measured using the multi-plate reader.

CHO cell culture and cytosolic Ca²⁺ level measurement. We tested whether the mutations could affect cytosolic Ca²⁺ levels by ET-1 compared to the wild type using Fura-2-AM, which is a cytosolic Ca²⁺-sensitive fluorescent dye. The procedure to measure the variations in cytosolic Ca²⁺ levels was adapted from a previous method³⁷. The genes of wild type and mutant ET_A in the pP9 vector were subcloned into the pCMVTag3B mammalian expression vector. The genes were amplified by PCR using a primer set (5'-gaggatctgagccggcgatccgattataaagtatgatgataaaatggaacccttgcctcagggc-3' and 5'-aggtaccggccccctcagtcattagctatgctgccttatggc-3'). The PCR products were ligated into the pCMVTag3B vector using *Bam*HI and *Hind*III restriction endonuclease sites by the Gibson cloning method. CHO-K1 cells from the American Type Culture Collection (USA) were cultured at 37 °C in a 5% CO₂ humidified incubator, and maintained in Ham's F-12 nutrient mix, GlutaMAX media supplemented with 10% (v/v) FBS, and 1x antibiotic-antimycotic solution in a 6-well cell culture plate until the cells reached 80% confluence. 2.5 μg of plasmids containing the mutant or wild type ET_A was transfected into the cells in each well using Lipofectamine 2000. After harvesting trypsin-digested cells by centrifugation at 200 × g for 3 min, the cells were resuspended in HEPES-buffered medium (HBM) consisting of 20 mM HEPES pH7.4, 103 mM NaCl, 4.8 mM KCl, 1.2 mM KH₂PO₄, 1.2 mM MgSO₄, 0.5 mM CaCl₂, 25 mM NaHCO₃, and 15 mM glucose; the cells were then incubated at room temperature with 5 μM Fura-2-AM for 40 min. After addition of 1 μM ET-1 to the 10⁵ transfected cells, the emissions at 510 nm for two excitation wavelengths (340 nm and 380 nm) were recorded for 100 sec using a fluorescence spectrophotometer (FS-2, Scinco, USA). The cytosolic Ca²⁺ level was evaluated by obtaining the ratio of the average fluorescence intensity excited at 340 nm to the intensity excited at 380 nm.

Real-time PCR. After preparation of the total RNA of CHO-K1 cells harboring each ET_A mutant or wild type ET_A, the complementary DNA (cDNA) was obtained by reverse transcription-PCR using an ET_A gene-specific primer set (5'-gcagaagtctcgtg-3' and 5'-ccaatc gctcaggaatg-3') and 110 ng of total RNA. The cDNA was amplified by PCR with SYBR green dye, and the signals of SYBR green incorporated into double-stranded DNA were monitored by a CFX96 Real-Time PCR detection system (Bio-Rad, USA).

References

- Wolfe, B. L. & Trejo, J. Clathrin-dependent mechanisms of G protein-coupled receptor endocytosis. *Traffic* **8**, 462–470 (2007).
- Tautermann, C. S. GPCR structures in drug design, emerging opportunities with new structures. *Bioorg. Med. Chem. Lett.* **24**, 4073–4079 (2014).
- Lappano, R. & Maggiolini, M. G protein-coupled receptors: novel targets for drug discovery in cancer. *Nat. Rev. Drug Discov.* **10**, 47–60 (2011).
- Geschwinder, S., Ulander, J. & Johansson, P. Ligand binding thermodynamics in drug discovery: Still a hot tip? *J. Med. Chem.* **58**, 6121–6335 (2015).
- Holdgate, G. A. Thermodynamics of binding interactions in the rational drug design process. *Expert Opin. Drug Discov.* **2**, 1103–1114 (2007).
- Freire, E. A. A thermodynamic approach to the affinity optimization of drug candidates. *Chem. Biol. Drug Des.* **74**, 468–472 (2009).
- Ferenczy, G. G. & Keseru, G. M. Enthalpic efficiency of ligand binding. *J. Chem. Inf. Model.* **50**, 1536–1541 (2010).
- Garbett, N. C. & Chaires, J. B. Thermodynamic studies for drug design and screening. *Expert Opin. Drug Discov.* **7**, 299–314 (2012).
- Klebe, G. Applying thermodynamic profiling in lead finding and optimization. *Nat. Rev. Drug Discov.* **14**, 95–110 (2015).
- Freire, E. Do enthalpy and entropy distinguish first in class from best in class? *Drug Discov. Today* **13**, 869–874 (2008).
- Olsson, T. S., Williams, M. A., Pitt, W. R. & Ladbery, J. E. The thermodynamics of protein-ligand interaction and solvation: insights for ligand design. *J. Mol. Biol.* **384**, 1002–1017 (2008).
- Ladbury, J. E., Klebe, G. & Freire, E. Adding calorimetric data to decision making in lead discovery: a hot tip. *Nat. Rev. Drug Discov.* **9**, 23–27 (2010).
- Kawasaki, Y. & Freire, E. Finding a better path to drug selectivity. *Drug Discov. Today* **16**, 985–990 (2011).
- Katritch, V., Cherezov, V. & Stevens, R. C. Structure-function of the G-protein-coupled receptor superfamily. *Annu. Rev. Pharmacol. Toxicol.* **53**, 531–556 (2013).
- Hynynen, M. M. & Khalil, R. A. The vascular endothelin system in hypertension – Recent patients and discoveries. *Recent Pat. Cardiovasc. Drug Discov.* **1**, 95–108 (2006).
- Said, N., Smith, S., Sanchez-Carbayo, M. & Theodorescu, D. Tumor endothelin-1 enhances metastatic colonization of the lung in mouse xenograft models of bladder cancer. *J. Clin. Invest.* **121**, 132–147 (2011).
- Kim, S.-J. *et al.* Macitentan, a dual endothelin receptor antagonist, in combination with temozolomide leads to glioblastoma regression and long-term survival in mice. *Clin. Cancer Res.* **21**, 4630–4641 (2015).
- Bagnato, A. & Natali, P. G. Endothelin receptors as novel targets in tumor therapy. *J. Transl. Med.* **2**, 16–24 (2004).
- Rosanò, L., Spinella, F. & Bagnato, A. Endothelin 1 in cancer: biological implications and therapeutic opportunities. *Nat. Rev. Cancer* **13**, 637–651 (2013).
- Adachi, M., Furuichi, Y. & Miyamoto, C. Identification of a ligand binding site of the human endothelin-A receptor and specific regions required for ligand selectivity. *Eur. J. Biochem.* **220**, 37–43 (1994).
- Breu, V. *et al.* Separable binding sites for the natural agonist endothelin-1 and the non-peptide antagonist bosentan on human endothelin-A receptors. *Eur. J. Biochem.* **231**, 266–270 (1995).
- Orry, A. J. W. & Wallace, B. A. Modeling and docking the endothelin G-protein-coupled receptor. *Biophys. J.* **79**, 3083–3094 (2000).
- Bhatnagar, S. & Rao, G. S. Molecular modeling of the complex of endothelin-1 (ET-1) with the endothelin type A (ET_A) receptor and the rational design of a peptide antagonist. *J. Biomol. Struct. Dyn.* **17**, 957–964 (2000).
- Lättig, J., Oksche, A., Beyersmann, M., Rosenthal, W. & Krause, G. Structural determinants for selective recognition of peptide ligands for endothelin receptor subtypes ET_A and ET_B. *J. Pept. Sci.* **15**, 479–491 (2009).
- Lee, K. *et al.* Purification and characterization of recombinant human endothelin receptor type A. *Protein Express. Purif.* **84**, 14–18 (2012).
- Na, J. H. *et al.* Bacterially expressed human serotonin receptor 3A is functionally reconstituted in proteoliposomes. *Protein Express. Purif.* **88**, 190–195 (2013).
- Han, S.-G. *et al.* An amphipathic polypeptide derived from poly-γ-glutamic acid for the stabilization of membrane proteins. *Protein Sci.* **23**, 1800–1807 (2014).
- Han, S.-G., Baek, S.-I., Lee, W.-K., Sudakar, P. & Yu, Y. G. Overexpression and functional stabilization of recombinant human lysophosphatidic acid receptor 1 using an amphipathic polymer. *B. Korean Chem. Soc.* **38**, 63–69 (2017).
- Simonson, M. S. & Dunn, M. J. Cellular signaling by peptides of the endothelin gene family. *FASEB J.* **4**, 2989–3000 (1990).
- Doi, T., Sugimoto, H., Arimoto, I., Hiroaki, Y. & Fujiyoshi, Y. Interactions of endothelin receptor subtype A and B with G_i, G_o, and G_q in reconstituted phospholipid vesicles. *Biochemistry* **38**, 3090–3099 (1999).

31. Shraga-Levine, Z. & Sokolovsky, M. Functional coupling of G proteins to endothelin receptors is ligand and receptor subtype specific. *Cell. Mol. Neurobiol.* **20**, 305–317 (2000).
32. Shihoya, W. *et al.* Activation mechanism of endothelin ET_B receptor by endothelin-1. *Nature* **537**, 363–368 (2016).
33. Fromant, M., Blanquet, S. & Plateau, P. Direct random mutagenesis of gene-sized DNA fragments using polymerase chain reaction. *Anal. Biochem.* **224**, 347–353 (1995).
34. Gibson, D. G. *et al.* Enzymatic assembly of DNA molecules up to several hundred kilobases. *Nat. Methods* **6**, 343–345 (2009).
35. Jung, S. J. *et al.* Aglycosylated IgG variants expressed in bacteria that selectively bind Fc γ RI potentiate tumor cell killing by monocyte-dendritic cells. *Proc. Natl. Acad. Sci. USA* **107**, 604–609 (2010).
36. Vukoti, K. M. *et al.* Molecular dissection of the interaction between hBLT2 and the G protein alpha subunits. *B. Korean Chem. Soc.* **28**, 1005–1009 (2007).
37. Park, S.-J. *et al.* Lysophosphatidylethanolamine utilizes LPA1 and CD97 in MDA-MB-231 breast cancer cells. *Cell. Signal.* **25**, 2147–2154 (2013).

Acknowledgements

This work is supported by a grant from the Global Ph.D. Fellowship Program (NRF-2013-034294), the Pioneer Research Center Program (NRF-2014M3C1A3051460), and the Mid-career Research Program (NRF-2016R1A2B4009952) through the National Research Foundation of Korea (NRF).

Author Contributions

S.-G.H., S.T.J. and Y.G.Y. designed experiments, analyzed the data and wrote the manuscript. S.-G.H., S.K. and W.-K.L. performed experiments.

Additional Information

Supplementary information accompanies this paper at doi:[10.1038/s41598-017-08096-6](https://doi.org/10.1038/s41598-017-08096-6)

Competing Interests: The authors declare that they have no competing interests.

Publisher's note: Springer Nature remains neutral with regard to jurisdictional claims in published maps and institutional affiliations.



Open Access This article is licensed under a Creative Commons Attribution 4.0 International License, which permits use, sharing, adaptation, distribution and reproduction in any medium or format, as long as you give appropriate credit to the original author(s) and the source, provide a link to the Creative Commons license, and indicate if changes were made. The images or other third party material in this article are included in the article's Creative Commons license, unless indicated otherwise in a credit line to the material. If material is not included in the article's Creative Commons license and your intended use is not permitted by statutory regulation or exceeds the permitted use, you will need to obtain permission directly from the copyright holder. To view a copy of this license, visit <http://creativecommons.org/licenses/by/4.0/>.

© The Author(s) 2017